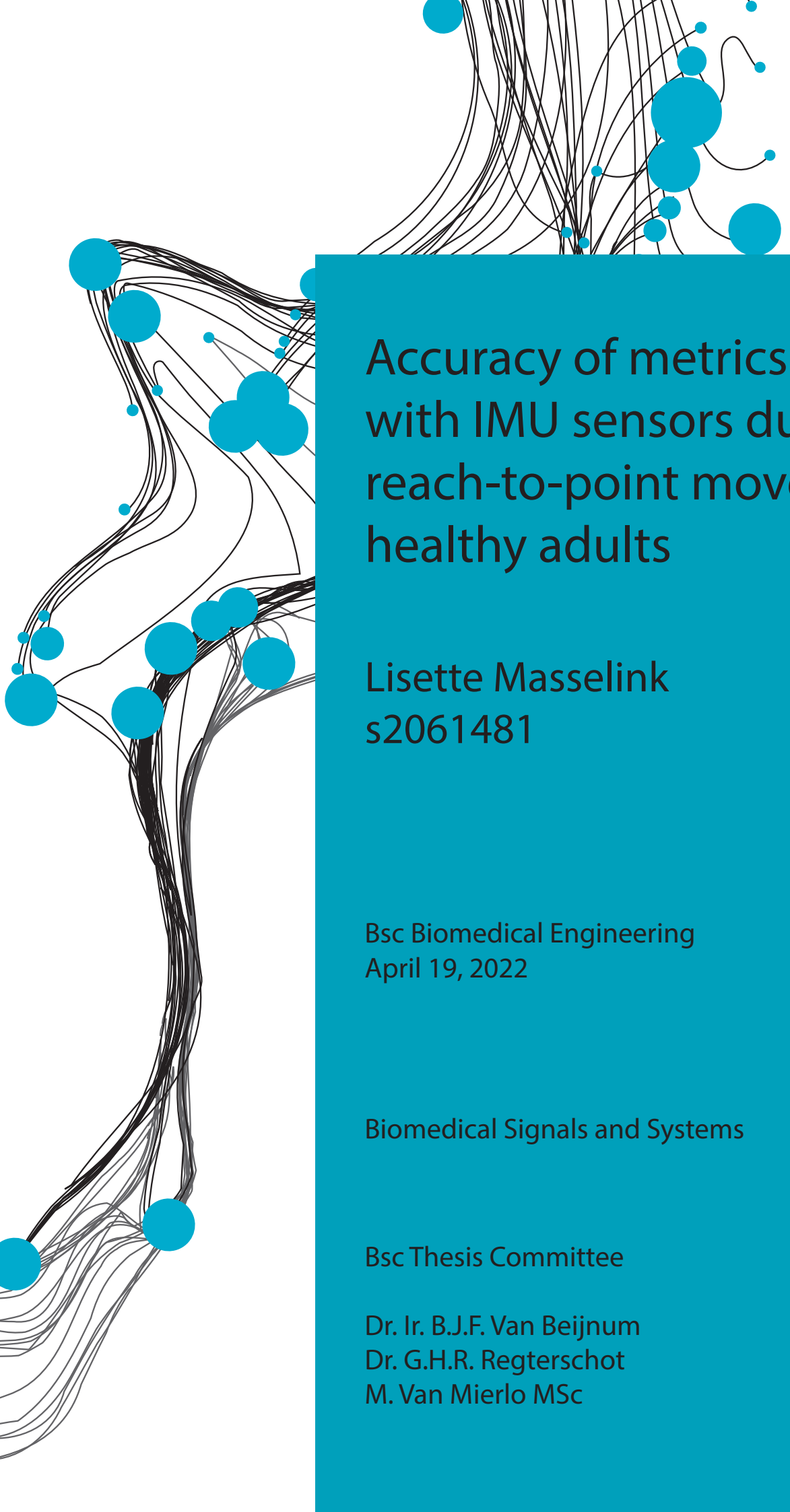

Accuracy of metrics measured with IMU sensors during a reach-to-point movement in healthy adults

Lisette Masselink
s2061481

Bsc Biomedical Engineering
April 19, 2022

Biomedical Signals and Systems

Bsc Thesis Committee

Dr. Ir. B.J.F. Van Beijnum
Dr. G.H.R. Regterschot
M. Van Mierlo MSc

Abstract

English

After a Cerebral Vascular Accident (CVA), intensive arm training can improve arm function. Using Inertial Measurement Units (IMUs), movement quality and compensatory movements can be captured. In this study, the accuracy of a system of nine IMUs is investigated during a reach-to-point movement in healthy adults. Three subjects reached to a cylindrical object and touched it briefly using three stroke compensation movements: trunk flexion, shoulder abduction and shoulder elevation. The results are evaluated by comparison with Vicon, an optical motion capture system. This study indicates that IMU based human motion analysis cannot provide accurate kinematic assessment of the of shoulder abduction, trunk flexion and reaching distance.

Nederlands

Na een cerebrovascular accident (CVA) kan de armfunctie worden verbeterd met behulp van intensieve training van de armen. Bewegingskwaliteit en compensatoire bewegingen kunnen worden vastgelegd door Inertial Measurement Units (IMU's). In deze studie is de accuraatheid van een systeem bestaand uit negen IMU's onderzocht tijdens een reikbeweging bij gezonde volwassenen. De drie proefpersonen reikten naar een cylindrisch object en raakten het vervolgens kort aan tijdens het uitvoeren van drie compensatoire bewegingen: rompflexie, schouderabductie en schouderelevatie. De resultaten zijn vergeleken met Vicon, een optisch systeem voor het vastleggen van bewegingen. Uit deze studie is gebleken dat bewegingsanalyse met behulp van IMU's geen accurate kinematische beoordeling van schouderabductie, rompflexie and reikafstand kan geven.

Contents

List of acronyms

CVA	Cerebral Vascular Accident
DALYs	Disability Adjusted Life Years
H	Hand
IMUs	Inertial Measurement Units
LA	Lower Arm
LOA	limits of agreement
MAE	mean absolute error
MARG	Magnetic, Angular Rate and Gravity
RMSE	root-mean-square error
ROM	range of motion
SD	standard deviation
SH	Shoulder
ST	Sternum
UA	Upper Arm

Chapter 1

Introduction

1.1 Problem Statement

Stroke, or a CVA, occurs when the blood supply to part of the brain is disrupted. Brain cells do not get enough oxygen and therefore die. There are two types of strokes: an ischaemic CVA, in which a blood clot obstructs the arteries in the brain, and a haemorrhagic CVA, in which a blood vessel bursts and blood flows into the brain. This results in a sudden onset of symptoms of focal failure in the brain [1] [2].

A CVA is one of the most common causes of disability and causes a large burden of disease. Between 1990 and 2019, the prevalence of a CVA increased by 85 percent, the mortality rate by 43 percent. The Disability Adjusted Life Years (DALYs) due to a CVA have increased by 32 percent. Thus, more and more people have to learn to live with the consequences of a CVA. 60 percent of CVA patients have permanent neurological problems with impaired motor skills. This limits their independence in daily life [3][4].

Hemiparesis, unilateral muscle weakness or paralysis, is common after a stroke. Sensory and motor function is impaired as cell death of neurons and supporting cells occurs in the centre of the infarct. Recovery occurs through adaptation, regeneration, and neuroplasticity. Neuroplasticity is the most important process, involving remapping of sensory and motor function from the damaged cells [5][6].

In CVA patients, muscle synergies change. A muscle synergy is a spatio-temporal pattern of activity across different muscles involved in performing a movement. Muscle synergies change as healthy synergies are disrupted, followed by new synergies through alternative descending pathways. After a CVA, two abnormal synergies of the upper extremities are often seen in the chronic phase, namely flexor synergy and extensor synergy. Flexor synergy is characterized by shoulder abduction with elbow flexion, supination and wrist and finger flexion. Extensor synergy is characterized by shoulder adduction, elbow extension, and pronation [7]. These synergies can cause neuromuscular control to be limited [8].

Rehabilitation can reduce the problems created by a stroke by stimulating neuroplasticity. Intensive arm training can improve arm motor function in both the acute and subacute phases after stroke. Measured effects on arm motor recovery are apparent after two hours of training per week [9][10]. The Fugl-Meyer Assessment (FMA) and the Action Research Arm Test (ARAT) are widely used to assess motor function. These tests, however, are insufficiently sensitive to capture the quality of sensorimotor function through the ordinal scales, and have a ceiling effect. Using these tests, it is not possible to distinguish recovery of movements from compensatory movements. By using objective metrics, both movement quality and compensatory movements can be captured [11] [12].

Inertial Measurement Units (IMUs) can be used for a kinematic analysis of arm movements. An IMU contains an accelerometer and a gyroscope. An accelerometer measures the acceleration of an object, and a gyroscope measures the angular velocity [13]. Performance of patients can be provided with immediate feedback using IMUs. A new generation of IMUs, which are low cost, wireless and simple to use, can be used for different applications such as home-based training [14][15]. Research has shown that a system of nine IMUs, placed on the chest, both shoulders, upper and lower arms, and hands, can distinguish movements of the affected and unaffected upper extremity of CVA patients. It was also possible to identify pathological muscle excitations and measure features related to pathological synapses [12]

Currently, it is unclear with what accuracy metrics measured with sensors can be determined during arm movements [11]. How accurately metrics can be measured with sensors depends on sensor placement, sensor measurement errors, sensor-to-segment calibration, and drift (due to integration of gyroscope data) and how you correct for them [14].

In the ArmCoach4Stroke project, it is important to investigate the accuracy of metrics during arm movements measured with sensors. The sensors will be used during the measurement of arm exercises in CVA patients in the home situation. Based on these measurements, the therapist can see how much and how well the patient is performing the arm exercises and can give feedback. The prerequisite for this is that the sensors provide sufficiently accurate measurements of metrics during arm exercises. Good accuracy means that relevant metrics can be determined with small measurement error, despite the high movement variability resulting from compensatory muscle synergies and segmented movements in stroke patients [14].

During a focus meeting of the ArmCoach4Stroke project, therapists indicated that relevant metrics during a reach-to-point movement are trunk flexion, shoulder abduction, shoulder elevation, reaching distance and smoothness. These metrics mainly show compensatory movements [11] Shoulder abduction and elbow extension are often seen in CVA-related abnormal muscle synergies. One of the compensatory strategies is trunk displacement to overcome the shoulder-elbow synergy [16].

This study focuses on investigating the accuracy of metrics measured with motion sensors during a reach to point movement in healthy adults. The accuracy of the metrics is determined by comparing the outcomes of the sensors to the gold standard (the Vicon system). The next step is to investigate the accuracy of metrics measured with motion sensors during a reach to point movement in CVA patients.

1.1.1 Research Question

The research question of this study is: *What is the accuracy of trunk flexion, shoulder abduction, and reaching distance measured with IMU sensors during a reach-to-point movement in healthy adults?*

Hypothesis

There will be a small deviation between the metrics measured with the IMU system and the Vicon system. This is because perfect positions are assumed in the calculation steps for the calibration of the IMUs. To calculate the metrics, integration steps are needed, which adds drift to the data. However, the accuracy will be good enough to provide feedback on the execution of arm exercises by patients.

Chapter 2

Methods

2.1 Study Design

The accuracy of trunk flexion, shoulder abduction, and reaching distance, measured with IMUs, is determined in this study. It is a qualitative cross-sectional study, performed in the mobility lab of Roessingh Research and Development (Enschede, The Netherlands).

2.2 Subjects

Eight subjects are recruited from University of Twente, The Netherlands. Criteria for selecting the subjects are as follows:

- Between 18 and 35 years old
- Right hand dominant
- No trunk, shoulder, arm, hand or finger injuries at the time of the measurement that may influence the performance of arm exercises

The subjects are instructed to perform some arm exercises. The experimental protocol is approved by the Ethics Committee of Computer & Information Science of the University of Twente and all subjects provided written informed consent prior to the measurements.

2.3 Measurement Setup

Nine IMU sensors (2M Engineering, $f_s = 50$ Hz) on the subject, an IMU sensor on a cylinder object ($f_s = 100$ Hz), a Vicon system (Vicon Motion Systems Ltd UK,$f_s = 100$ Hz) and two Rollei video cameras ($f_s = 100$ Hz) will be used to record a set of arm exercises.

The Vicon system, consisting of six high-speed infrared cameras, captures the three-dimensional position of the different markers in space. This is assumed as the gold standard for the kinematic data in this study [17]. Objects blocking the camera view or producing undesired reflections were removed from the measurement environment.

An overview of the experiment is shown in table 2.1. The experiment lasted two and a half hours per subject. For this study, only data of session 1 is analysed.

Table 2.1: Steps in experiment

Steps in experiment	Time duration (min)
1. Explanation of experiment and signing informed consent	5
2. Annotation of: age, gender. Measurement of body mass, length of arms, upper arm, lower arm, hands, and offsets	10
3. Attachment of 9 IMU sensors and 21 markers (for Vicon measurement) to subject	15
4. Sensor-to-segment calibration movements	10
5. Performance of arm exercises (session 1)	30
6. Removal of 9 IMU sensors	10
7. Attachment of 9 IMU sensors to subject	15
8. Sensor-to-segment calibration movements	10
9. Performance of arm exercises (session 2)	30
11. Removal of 9 sensors and Vicon markers	10
12. End of experiment and oral debriefing	5
Total time duration	**150**

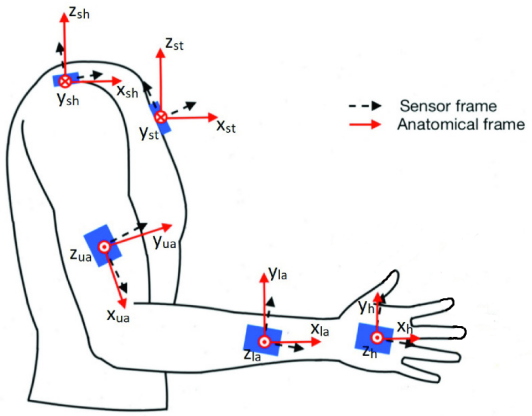

Figure 2.1: IMU attachment. Adapted from [12]

2.3.1 Attachment locations of the IMUs and markers

The IMU sensors are attached with medical tape on the skin on the following locations on the body (see figure 2.1[12]

- Sternum (ST): at the centre of the chest
- Shoulder (SH): on top of the acromion, between the superior border of the scapula and the clavicle, near the acromioclavicular joint
- Upper Arm (UA): lateral side, close to the elbow
- Lower Arm (LA): dorsal side, close to the wrist
- Hand (H): central on dorsal side

The 14 mm markers for the Vicon system were placed according to the Plug-in Gait Upper Body model (excluding the markers on the head), see figure 2.2 and appendix A [18]. Markers on the hand (RFIN and LFIN) and shoulders (LSHO and RSHO) were placed on top of the IMUs. Two additional markers were placed on both index fingers. The markers were attached with EMG stickers.

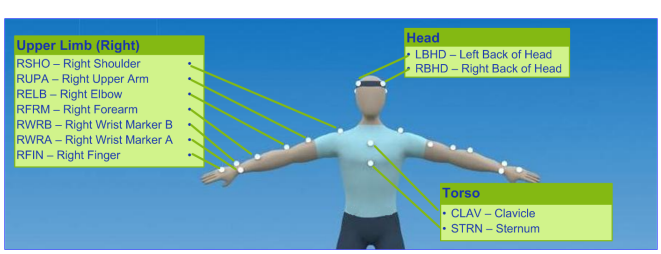

(a) Front view

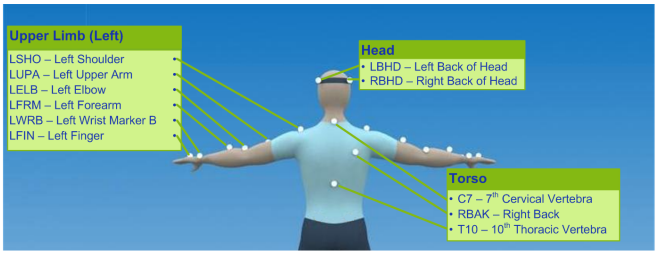

(b) Back view

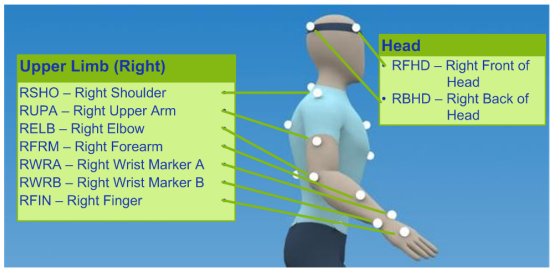

(c) Right side view

Figure 2.2: Marker placement on the upper body. The head markers were excluded. From [18]

2.3.2 Sensor-to-segment calibration

This sensor-to-segment calibration is important for the estimation of the joint angles based on the IMU-data. The IMU sensors will be aligned with the atomical segment frames using the functional alignment method (FMA), see table 2.2

Table 2.2: Sensor-to-segment calibration protocol to define the anatomical axes. Adapted from [12]

Calibration Position/Movement	Anatomical Axis
1. Hand flat on table (static) for 5 seconds	$\vec{z_h}$
2. Side of hand (ulna) on table with elbow 90 degrees flexion (static) for 5 seconds	$\vec{y_h}$
3. Lower arm and hand flat on table for 5 seconds (static)	$\vec{z_{la}}$
4. Wrist pronation, starting from supination position (dynamic movement): three times	$\vec{x_{la}}$
5. Shoulder adduction with elbow in 90 degrees flexion (static) for 5 seconds	$\vec{x_{ua}}$
6. Shoulder abduction with elbow in 90 degrees flexion (static) for 5 seconds	$\vec{z_{ua}}$
7. Standing straight in 'neutral pose' with arms straight along body pointing downward (static) for 5 seconds	$\vec{z_{sh}}$,$\vec{z_{st}}$
8. Trunk flexion movement with arms straight along body (dynamic movement): three times	$\vec{y_{sh}}$,$\vec{y_{st}}$
9. Sitting straight with arms straight along body pointing downward (static) for 5 seconds	$\vec{z_{sh}}$,$\vec{z_{st}}$
10. Trunk flexion while sitting, with arms straight along body (dynamic movement): three times	$\vec{y_{sh}}$,$\vec{y_{st}}$

2.3.3 Global frame definition

Prior to the exercises, the global frame is defined by the following movements (see figure 2.3):

- Sitting straight with arms along the body to define the common vertical axis using the gravity vector
- Trunk flexion with arms moving along the upper body to define the horizontal axis using the angular velocity

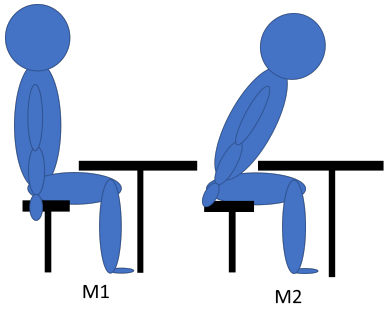

Figure 2.3: Movements used to define the global frame

This step is necessary to define the initial (start) orientation of the sensors. Using the Madgwick filter, it is then possible to estimate the next sensor orientations based on the initial orientation. The global frame definition is important for defining the initial orientation of the sensors in the global frame [12].

2.3.4 Arm exercises

The following arm exercises are performed:

1. Reach from the start position to a cylinder object and touch it briefly. The cylinder object stands on one of the four end positions (10 trials per end position)
2. Reach from the start position to the cylinder object and grasp it, move the object a bit upward, put the object back on its place on the table, move hand back to start position. The cylinder object stands on one of the four end positions (10 trials per position).
3. Reach from the start position, grasp, and transport the cylinder object from one place of the table to the other and back. Cylinder object stands on one of the four end positions.
    - Moving the object from the left end position to the right end position and back (10 trials).
    - Moving the object from the nearest end position to the farthest end position and back (10 trials).
4. Moving the palmar side of the hand over the back of the head 5 times (10 trials)
5. Imitating a stroke patient: reach, from the start position, to a cylinder object and touch it briefly. Movement will be performed combining three stroke compensation movements: trunk flexion, shoulder abduction and shoulder elevation (10 trials), see figure 2.4

The subjects are sitting on a crutch next to a table which are adjustable in height. The knees are at 90 degrees, and the elbow at 90 degrees when the hand is resting on the edge of the table, without shoulder elevation. All exercises are performed at a self-preferred movement speed, first with the dominant right arm, then with the left arm. There are four positions for the cylinder object in the experiment, see figure 2.5.

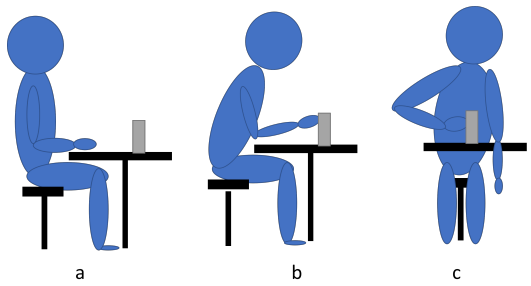

Figure 2.4: Illustration of exercise 5, with the begin position (a) and the reaching movement with trunk flexion and shoulder abduction (b, c)

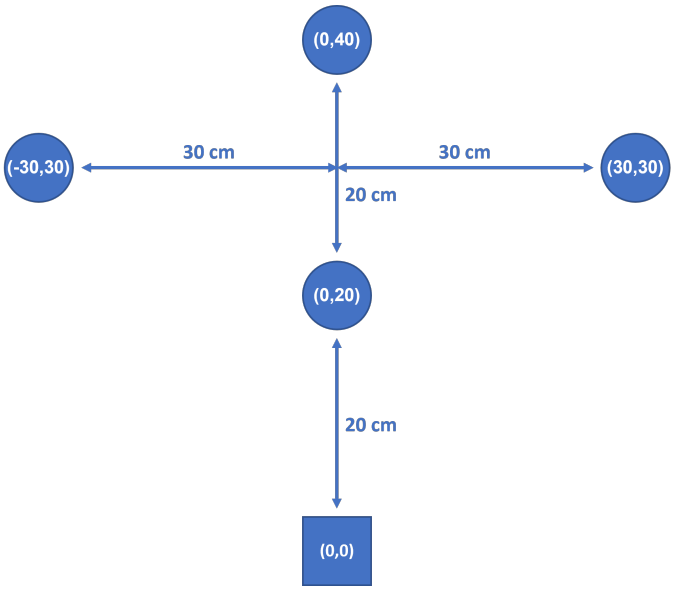

Figure 2.5: Set up of the experiment. (0,0) is the starting position of the hand of the subject. The hand is in the centre line of the trunk and 5 cm from the edge of the table. The cylindric object can be on four different positions, namely 1(0,40), 2(30,30), 3(0,20) and 4(30,30)

2.4 Data Processing

Data collection of the IMUs on the subject was done using a PC software tool (2M Engineering). Data collection of the IMU in the cylinder object was done using Matlab 2022a (Mathworks, Inc., Natick, MA, USA). All data processing and the statistical analysis are performed in Matlab 2022a (The Mathworks Incl.). Data of the IMUs and Vicon system are resynchronized using cross-correlation. For this, Vicon data were resampled at 50 Hz to be easily compared to the IMU data. Both Vicon and IMU signals were filtered by a second order Butterworth low-pass filter with a cut-off frequency of 20 Hz to remove high frequency noise [19].

2.4.1 IMUs

An IMU consists of a gyroscope and an accelerometer. For further analysis of this data, a few steps are necessary, namely sensor-to-segment calibration, defining the global frame, estimation of the orientation and extraction of the joint angles [12].

First, some calibration corrections are performed on the accelerometer and gyroscope data, whereafter some zero-velocity updates are performed to remove noise from gyroscope data. Then the accelerometer

and gyroscope data are filtered.

Sensor-to-segment calibration

The sensor-to-segment calibration is necessary to find the orientation of the sensor with respect to the corresponding the body segment. The axis of the anatomic frame of the corresponding body segment is determined by the gravity vector in the static posture. The x-axis of the anatomic frames of the hands and arms are in the longitudinal direction of these segments. In the static neural pose, the following axes are determined: $\vec{x_h}$, $\vec{x_{la}}$, $\vec{x_{ua}}$, $\vec{z_{sh}}$ and $\vec{z_{st}}$. The other axes are determined using the angular velocity during a dynamic movement. The following axes are determined using the dynamic movement: $\vec{z_h}$, $\vec{z_{la}}$, $\vec{z_{ua}}$, $\vec{y_{sh}}$ en $\vec{y_{st}}$. For each sensor, two axes are measured, whereafter the third axis can be calculated using the cross-product. To ensure that the axis are orthogonal, one axis will be redefined using the cross product. The accelerometer data during the static movements and the gyroscope data during the static movements are filtered using a median filter to remove noise [12].

The orientation of the coordinate system of the segment with respect to the sensor is given by the rotation matrix shown in equation 2.1 [12].

$$^{S}R_{seg} = \begin{bmatrix} \vec{x_{seg}} & \vec{y_{seg}} & \vec{z_{seg}} \end{bmatrix} \tag{2.1}$$

Global frame definition

The next step is to estimate the initial orientation of the sensors in the body frame. This is the initial orientation as measured during the neutral pose. The x-axis corresponds to the frontal axis, the y-axis to the sagittal axis, and the z-axis to the longitudinal axis. In this step, $^{G}R_s$ in the initial position is determined.

Orientation estimation

The orientation change from the initial orientation to the starting position is calculated, whereafter the sensor orientating during exercises starting in de start position is estimated. To estimate the orientation, the angular velocity is integrated. This is performed using a Madgwick filter using the gyroscope and accelerometer data to compensate for the integration drift.

The Madgwick filter is used to determine the orientations of the IMU sensors in the global frame based on the initial orientation in the global frame. First, the filter is used to estimate the orientation change from initial orientation to starting position, whereafter it is also used to estimate the sensor orientations during exercises starting in the start position [20].

The orientation of a body segment in the global frame can be calculated using equation [20] 2.2

$$.^{G}R_{seg}(t) =^{G} R_s(t)^{S}R_{Seg} \tag{2.2}$$

Determine start and end of reaches

The start and end of reaches are determined in hand accelerometer data, see figure 2.6. The start point is the last point in a certain range from the marked point when the normalized acceleration of the hand IMU is less than the value at the marked point plus the value of the median plus 0.05 m/s^2. The end point is the point when the acceleration signal first crosses zero again after the negative peak.

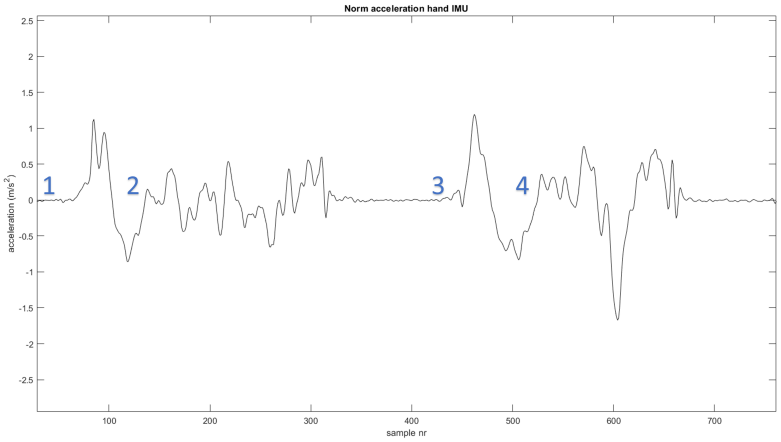

Figure 2.6: Determination of the start and end of two reaches using the normalized acceleration of the hand IMU. 1 and 2 are the marked start and end points for the first reach, 3 and 4 for the second reach

Joint angles

The joint angles are calculated using the orientation of the body segments. The first step in calculating the joint angle is projecting a certain vector $\vec{v}$ on a certain frame (with normal vector $\vec{n}$), for which equation 2.3 is used.

$$\vec{v^p} = \vec{v} - \frac{\vec{v} \cdot \vec{n}}{||\vec{n^2}||}\vec{n} \tag{2.3}$$

The following step is to calculate the angle between two vectors, using equation 2.4

$$\theta = atan2\Big(\frac{||\vec{v_1} \times \vec{v_2}||}{\vec{v_1} \cdot \vec{v_2}}\Big) \tag{2.4}$$

The trunk flexion angle was determined using the x-coordinate of the sternum and shoulders, see figure 2.7a. The shoulder abduction/adduction angle was calculated by projecting $\vec{x_{ua}}$ on the zy-plane (frontal plane) of the shoulders, whereafter the angle between $\vec{x^p_{ua}}$ en $\vec{y_{sh}}$ was determined, see figure 2.7b.

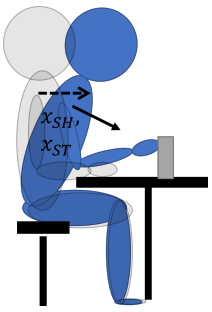

(a) Trunk flexion angle

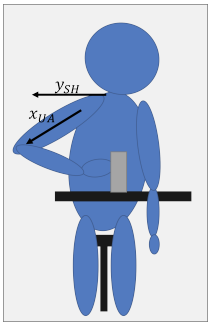

(b) Shoulder abduction angle

Figure 2.7: Trunk flexion is calculated using the angle between the x-axis (solid arrow) of the sternum $\vec{x_{st}}$ or shoulder $\vec{x_{sh}}$ with respect to the x-axis before the movement (dashed arrow). To calculate shoulder abduction, the x-axis of the upper arm $\vec{x_{ua}}$ is projected in the frontal plane (grey area), whereafter the angle between $\vec{x^p_{ua}}$ and $\vec{y_{sh}}$ is determined

Reaching distance

The reaching distance is calculated by some integration steps. The first step is to remove the gravity of the vertical acceleration (2.5).

$$a = \begin{bmatrix} a_x & a_y & a_z - 9,81 \end{bmatrix} \tag{2.5}$$

Then, the velocity is calculated by integrating the acceleration (2.6), followed by correction for the integration drift by assuming constant noise. To calculate the velocity drift, velocity is assumed to be zero at start and end of the movement.

$$v(t) = v(t-1) + a(t)dt \tag{2.6}$$

The reaching distance is calculated by integrating the compensated velocity (2.7.

$$d(t) = d(t-1) + v_{com}(t)dt \tag{2.7}$$

The total reaching distance is equal to the distance in the x-, y- and z-direction (2.9)

$$d = \begin{bmatrix} d_x & d_y & d_z \end{bmatrix} \tag{2.8}$$

$$|d| = \sqrt{d_x^2 + d_y^2 + d_z^2} \tag{2.9}$$

2.4.2 Vicon

The optical kinematic data was modelled using the Plug-in Gait Upper Body model. The position of the markers was captured by six high-speed cameras. The data was collected and labeled using Vicon Nexus 2.12 (Vicon Motion Systems Ltd UK.). A minimum of two cameras are required to start and continue a trajectory.

Gapfilling of markers on the upper limb was performed using a Dynamic BodyLanguage Model which uses the 5 marker rigid body cluster with missing markers 'C7', 'T10', 'CLAV', 'STRN' and 'RBAK' during a dynamic trial. For all markers, gap filling is performed using Woltring quintic spline interpolation with a maximum gap length of 10 frames.

A static model is run to calculate certain static values required for the dynamic modelling. Using the dynamic Plug-in Gait model, positions of joints and angles between joints are calculated. The positions of the rigid segments are defined on frame-by-frame basis.

Kinematics

The global (laboratory) co-ordinate system is defined with the z-axis perpendicular to the lab floor (vertical) and the x-and y-axes in the plane of the lab floor, with the x-axis in the longitudinal direction.

The chord function is used to calculate the shoulder joint centre, the elbow joint centre and the hand joint centre. The chord function uses three points, a previously calculated joint centre, a real marker at a known offset from the required joint centre, and another point or marker, to define a plane [18]. An illustration of the chord function can be seen in figure 2.8.

Thorax

The z-axis of the thorax is the direction from the midpoint of STRN and T10 to the midpoint of CLAV and C7. The x-axis points forwards and is defined from the midpoint of C7 and T10 to the midpoints of CLAV

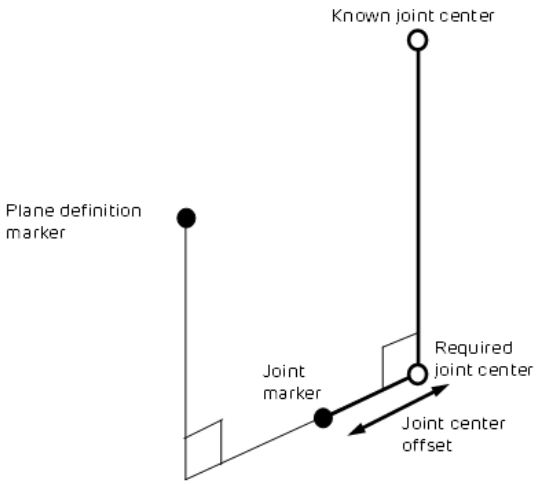

Figure 2.8: Chord function. From [18]

and STRN. The y-axis is calculated using the cross product and points leftwards. The origin is calculated from the CLAV marker with an offset of half a marker diameter along the x-axis [18].

Shoulder

The shoulder joint centre is defined as the origin for each clavicle. First, the virtual shoulder 'wand' marker is defined using a direction perpendicular to the line from the thorax origin to the SHO marker, and the thorax x-axis. The shoulder 'wand' marker is defined using this direction. The shoulder joint centre is calculated using the chord function, with inputs shoulder offset, thorax origin, shoulder marker and shoulder 'wand' [18].

Clavicle

The z-axis of the clavicle is defined from the direction from the joint centre to the thorax origin. The x-axis is the shoulder 'wand' direction and points forwards. The y-axis of the right clavicle points downwards, the y-axis of the left upwards [18].

Elbow

The direction of a construction vector is perpendicular to the plane defined by the shoulder joint centre, the elbow marker (ELB) and the midpoint of the two wrist makers (WRA and WRB). The elbow joint centre is defined using the chord function using the shoulder joint centre, the elbow marker and the midpoint of the two wrist markers [18].

Wrist

The wrist joint centre is determined as an offset from the midpoint of the wrist markers along a line perpendicular to the line along the wrist bar, and the line joining the wrist bar midpoint to the elbow centre [18].

Humerus

The origin of the humerus is the elbow joint centre with the z-axis from elbow joint centre to the shoulder joint centre and the x-axis between the elbow joint centre and wrist joint centre [18].

Joint angles

Plug-in Gait uses Euler angles in rotation order YXZ to calculate joint angles. Trunk flexion is calculated using the angle between the thorax x-axis and the laboratory coordinate system. Shoulder angles are rel-

ative, namely the angle between the upper arm and thorax [18].

Reaching distance

Reaching distance is calculated using the three-dimensional difference between the start position and the maximum position in the longitudinal direction of the hand marker during reaching (2.10).

$$|d| = \sqrt{d_x^2 + d_y^2 + d_z^2} \tag{2.10}$$

2.4.3 Statistic analysis

Both maximum angles and range of motion (ROM) of shoulder abduction and trunk flexion will be analysed. Furthermore, reaching distance is evaluated.

The accuracy of the measurement system is the systematic difference between the measured average and the true value (bias) [21]. To assess the agreement of the two methods, root-mean-square error (RMSE), mean absolute error (MAE), and Pearson's correlation coefficient are used to quantify the agreement. For the RMSE and MAE, $<5^\circ$ was considered as excellent and between 5 and 10° as good [22]. For reaching distance, good RMSE and MAE is equal to 10% of the total range, meaning 0.04 m [23].

Pearson's correlation coefficient is used to determine linear correlation, which is categorized as weak (r $\leq$ 0.35), moderate (0.35 $<$ r $\leq$ 0.67), strong (0.67 $<$ r $\leq$ 0.90) and excellent (r $>$ 0.90)[24].

Because the Pearson's correlation coefficient does not account for systemic bias, the Bland-Altman analysis is also used [25]. The Bland-Altman analysis is used to describe agreement between the IMU and Vicon measurements, based on the limits of agreement. It results in a scatter plot XY, where the difference of the data is plotted on y-axis, the average of the measurements on the x-axis [26]. The difference is equal to $M1 - M2$, in which M1 is the value of the IMUs and M2 the value of Vicon. The limits of agreement (LOA) are defined as [27]:

$$LOA = mean \pm 1.96SD \tag{2.11}$$

For the limits of agreement, 10 $^\circ$ lower or upper LOA are acceptable for biomechanics applications, meaning a standard deviation (SD) of 5° [28].

Chapter 3

Results

Data from three participants (3 F, age 24.7 $\pm$ 3.2 years, length 169 $\pm$ 3.5 cm, weight 79.6 $\pm$ 18.2 kg) is analysed. For the subject measurements, see table 3.1. The arm length is measured from the acromion clavicular joint to the wrist joint. Upper arm length is measured from the acromion clavicular joint to the elbow joint. The lower arm length is measured from the elbow joint to the wrist joint. The hand length is measured from the wrist joint to the tip of the middle finger.

The shoulder offset is the vertical distance from the centre of the glenohumeral joint to the base of the marker on the acromion clavicular joint. The elbow width is measured along the flexion axis (between the medical en lateral epicondyles of the humerus). The wrist width is the anterior/posterior thickness of the wrist. The hand thickness is measured as the anterior/posterior thickness between the dorsum and palmar surfaces of the hand [18].

Table 3.1: Subject measurements (n=3)

Measurement	left	right
arm length (cm)	52.3 $\pm$ 2.7	50.6 $\pm$ 0.6
upper arm length (cm)	26.7 $\pm$ 2.5	27.1 $\pm$ 2.2
fore arm length (cm)	25.3 $\pm$ 1.2	24.9 $\pm$ 0.7
hand length (cm)	16.3 $\pm$ 0.6	15.0 $\pm$ 1.1
shoulder offset (mm)	50.7 $\pm$ 6.7	50.7 $\pm$ 8.1
elbow width (mm)	75.9 $\pm$ 4.5	74.9 $\pm$ 7.4
wrist width (mm)	35.2 $\pm$ 4.8	34.9 $\pm$ 4.2
hand thickness (mm)	23.7 $\pm$ 4.6	24.0 $\pm$ 6.1

3.1 Metrics

To assess the designed IMU-system, data of the IMUs was compared to the optical data (Vicon). Optical data was selected based on minimal marker occlusions. An example of the shoulder abduction and trunk flexion during exercise 5 can be seen in figure 3.1. Shoulder abduction and trunk flexion angles of all subjects are shown in appendix B. Data of each subject is shown in figure 3.2 to assess the variability. Data of range of motion of right shoulder abduction of subject two is excluded due to many marker occlusions.
The measured maximum angle and range of motion of shoulder abduction and trunk flexion are summarised in table 3.2. In this table, the measured reaching distance is also set out.

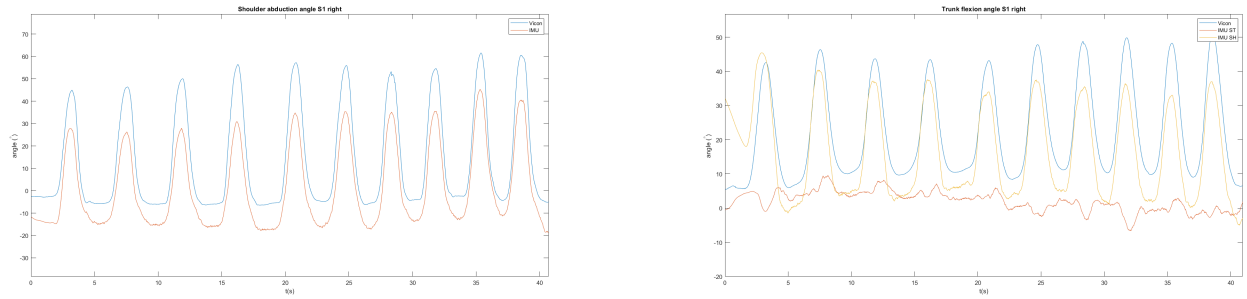

(a) Shoulder abduction angle

(b) Trunk flexion angle

Figure 3.1: Example of the shoulder abduction and trunk flexion angles during exercise 5. Vicon data are in blue. IMU data are a) in red and b) in red (measured with ST) and yellow (measured with SH).

Table 3.2: Results for performance of exercise 5, with bias and SD of the Bland-Altman analysis as percentage of the Vicon mean. IMU: inertial measurement unit; SD: standard deviaton; RMSE: root mean squared error; MAE: mean absolute error; Pearson's r: Pearson's correlation coefficient; $^{*}p < 0.05$, $^{**}p < 0.01$

Metrics	IMU		Vicon		RMSE	MAE	Pearson's r	Bland-Altman	
	Mean	SD	Mean	SD				Bias (%)	SD (%)
Shoulder abduction (°)									
Left	80.0	18.1	82.4	17.4	18.6	-2.8	0.45*	-2.8 (-3.4)	18.7 (22.7)
Right	71.0	26.8	80.0	19.8	13.2	-9.6	0.97**	-9.6 (-12.0)	9.2 (11.5)
Trunk flexion ST (°)									
Left	24.5	25.4	40.0	7.7	24.7	–15.5	0.83**	-15.5 (-38.8)	19.5 (48.8)
Right	20.3	15.0	41.7	5.8	26.4	-21.4	0.05	-21.4 (-51.3)	15.8 (38.8)
Trunk flexion SH (°)									
Left	34.2	8.4	40.0	7.7	9.9	-5.9	0.50**	-5.9 (-14.8)	8.1 (20.0)
Right	30.1	11.6	41.7	5.8	13.7	-11.6	0.84**	-11.6 (-27.8)	7.4 (17.7)
Shoulder abduction ROM (°)									
Left	82.0	21.5	70.8	10.9	24.7	10.0	0.11	10.0 (14.1)	23.1 (32.6)
Right	61.0	20.6	70.6	13.6	9.1	-2.2	0.94**	-2.2 (-3.1)	9.0 (12.7)
Trunk flexion ST ROM (°)									
Left	18.5	18.4	31.9	7.2	20.8	-13.4	0.49**	-13.4 (-42.0)	16.2 (50.8)
Right	21.1	13.4	34.2	8.3	18.3	-13.1	0.37*	-13.1 (-38.3)	12.9 (37.7)
Trunk flexion SH ROM (°)									
Left	26.6	6.9	31.9	7.2	12.3	-5.3	-0.27	-5.3 (-16.6)	11.2 (35.1)
Right	33.6	5.2	34.2	8.3	6.6	-0.7	0.60**	-0.7 (-2.0)	6.7 (19.6)
Reaching distance (m)									
Left	0.21	0.13	0.36	0.04	0.19	-0.14	0.50**	-0.14 (-38.9)	0.12 (33.3)
Right	0.27	0.14	0.34	0.04	0.13	-0.07	0.97**	-0.08 (-23.4)	0.11 (32.4)

3.2 RMSE and MAE

Root mean squared error (RMSE) and mean absolute error (MAE) are presented in table 3.2.

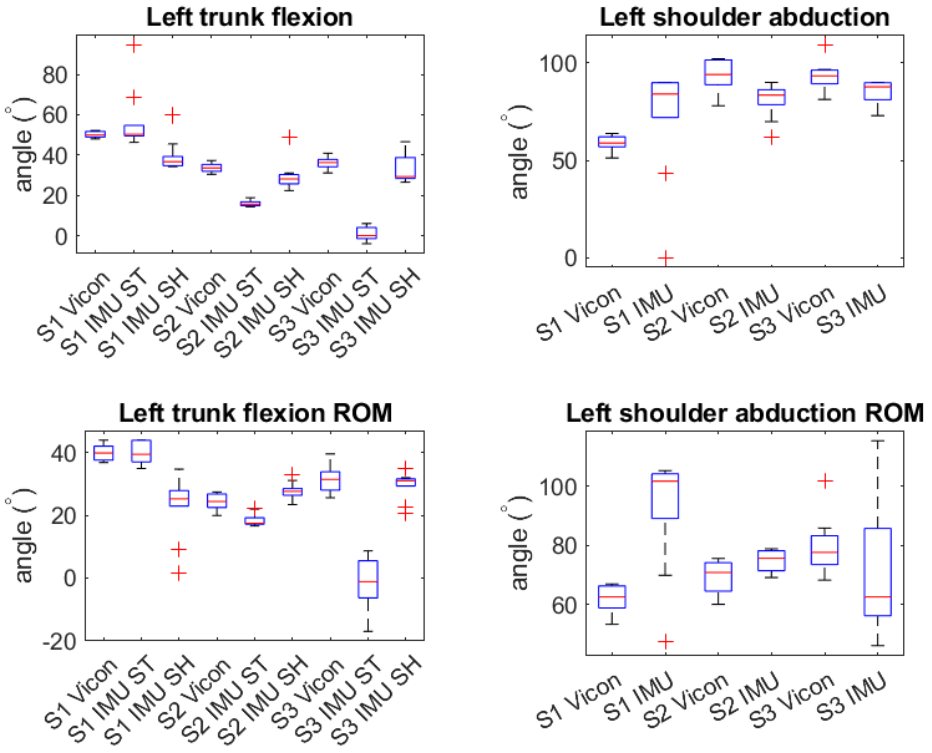

(a) Left hand

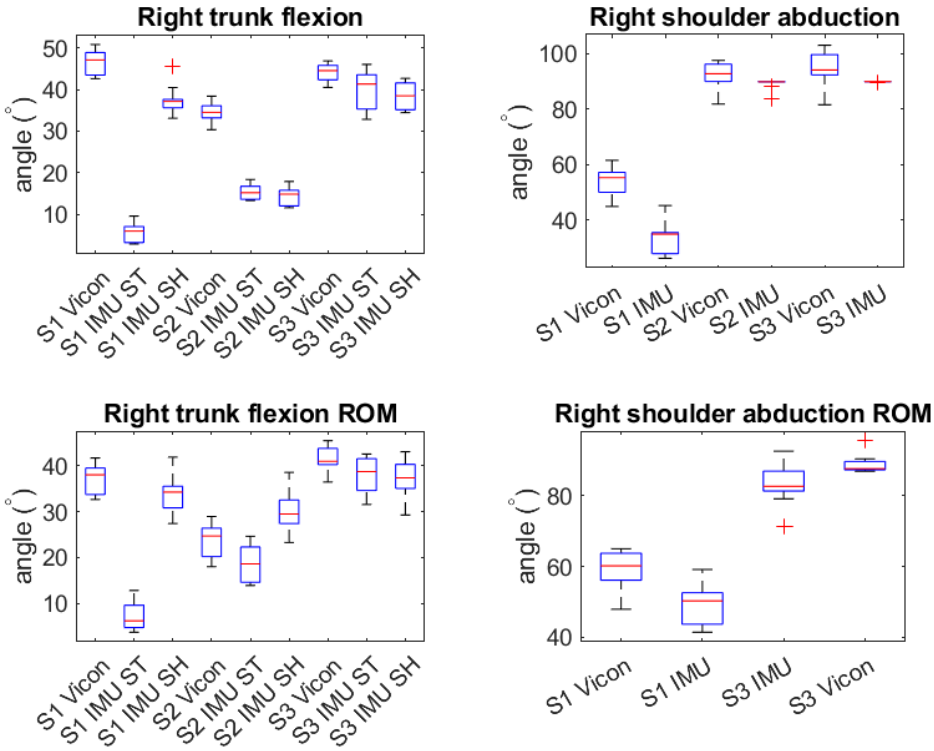

(b) Right hand

Figure 3.2: Boxplots of maximum angles and range of motion of trunk flexion, shoulder abduction and reaching distance of the exercises, performed with the left (a) and the right (b) hand

RMSE is not excellent for any of the metrics. However, it can be assessed as good for left trunk flexion measured with shoulder IMU, ROM of right shoulder abduction and ROM of right trunk flexion measured

with the shoulder IMU.

MAE is excellent for left shoulder abduction, ROM of right shoulder abduction and ROM of right trunk flexion measured with the shoulder IMU. MAE is good for left shoulder abduction, left trunk flexion measured with shoulder IMU and ROM of trunk flexion measured with shoulder IMU.

3.3 Pearson's r

From the data shown in table 3.2, it can be seen that there is an excellent correlation for right shoulder abduction and right shoulder abduction ROM. Correlation can be assessed as good for left trunk flexion measured with sternum IMU, right trunk flexion measured with shoulder IMU and right reaching distance.

Metrics which can be assessed with good correlation are trunk flexion measured with the sternum IMU for the left and trunk flexion measured with the shoulder IMU for the right.

3.4 Bland-Altman Analysis

The Bland-Altman plots to assess agreement between IMU and Vicon for maximum shoulder abduction and trunk flexion and the reaching distance are shown in figures 3.3 and 3.4. The Bland-Altman plot for range of motion of shoulder abduction and trunk flexion are shown in figures 3.5 and 3.6. Figure 3.7 shows the Bland-Altman plot for reaching distance.

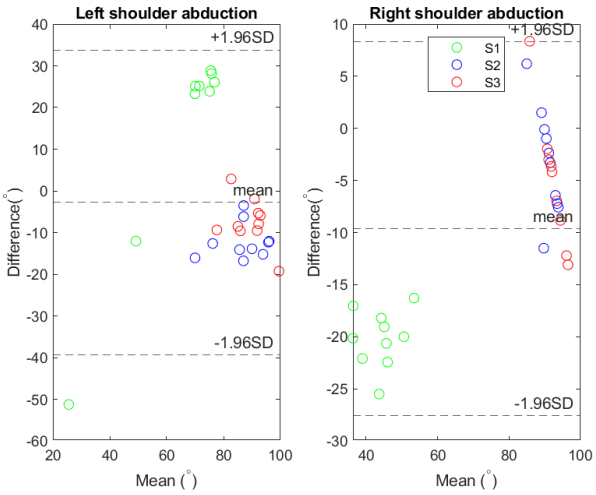

Figure 3.3: Bland-Altman plot of the maximal shoulder abduction angles for exercise five performed with the left hand (left) and the right hand (right). Data of subject 1 is indicated in green, data of subject 2 in blue and data of subject 3 in red.

The bias of the IMU system is relatively low for both maximum angles and ROM of shoulder abduction and trunk flexion measured with shoulder IMU. The bias is highest for both maximum angles and ROM of trunk flexion measured with the sternum IMU.

For all metrics, the plots demonstrated that the differences are within the limits of agreement, except for some outliers. Overall, the standard deviation and thus the limits of agreement for the metrics are relatively high.

Figure 3.4: Bland-Altman plot of the maximal trunk flexion angles for exercise five performed with the left hand (top) and the right hand (below), measured with the sternum (left) and shoulder (right) IMU. Data of subject 1 is indicated in green, data of subject 2 in blue and data of subject 3 in red.

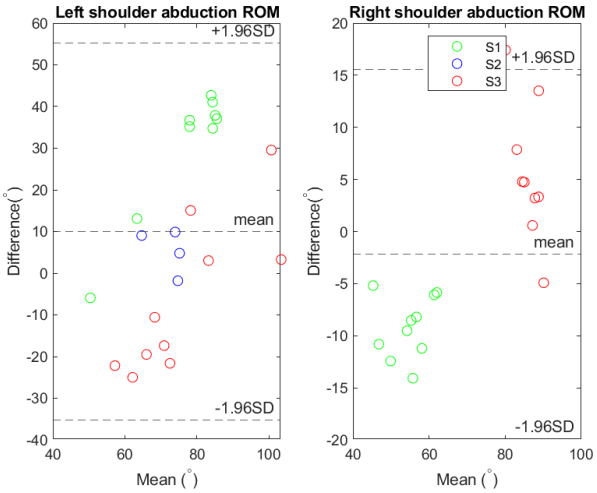

Figure 3.5: Bland-Altman plot of the range of motion of shoulder abduction angle for exercise five performed with the left hand (left) and the right hand (right). Data of subject 1 is indicated in green, data of subject 2 in blue and data of subject 3 in red.

Figure 3.6: Bland-Altman plot of the range of motion of trunk flexion angle for exercise five performed with the left hand (top) and the right hand (below), measured with the sternum (left) and shoulder (right) IMU. Data of subject 1 is indicated in green, data of subject 2 in blue and data of subject 3 in red.

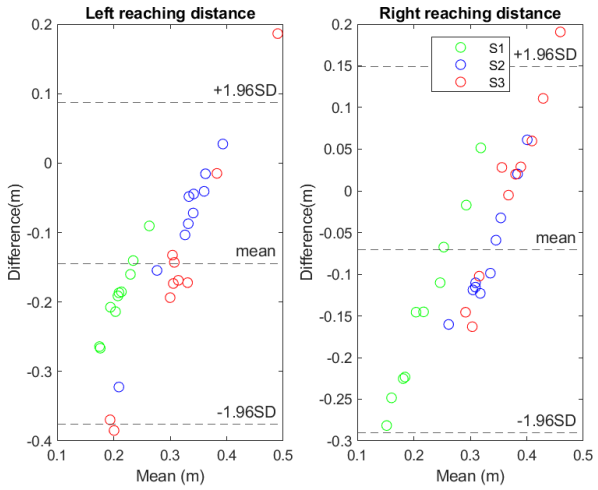

Figure 3.7: Bland-Altman plot of the maximum reaching distance for exercise five performed with the left hand (left) and the right hand (right). Data of subject 1 is indicated in green, data of subject 2 in blue and data of subject 3 in red.

Chapter 4

Discussion

4.1 Key findings and interpretation

The objective of this study was to determine the accuracy of both maximum angles and range of motion of shoulder abduction, trunk flexion and reaching distance measured with a system of IMUs. This study indicates that IMU based human motion analysis cannot provide accurate kinematic assessment of shoulder abduction, trunk flexion and reaching distance when compared to Vicon, the gold standard for kinematics, during a certain reach-to-point movement in healthy adults.

The RMSE and MAE varied between the different metrics. RMSE and MAE were only good for left trunk flexion measured with shoulder IMU and ROM of right trunk flexion measured with sternum IMU. The RMSE and MAE for trunk flexion measured with the shoulder IMU is lower than for trunk flexion measured with the shoulder IMU, which indicates the shoulder IMU is more accurate to measure trunk flexion.

Pearson's correlation coefficient ranged from 0.37 to 0.97. Correlation was only excellent or good for right shoulder abduction, range of motion of right shoulder abduction and right reaching distance.

In general, the IMU system underestimated all angles, with exception to range of motion of left shoulder abduction. A constant bias does not limit the use of the IMUs because it can be accounted for in the interpretation of the data [29]. The standard deviation and thus the limits of agreement are lowest for maximum and ROM of trunk flexion measured with shoulder IMU. Overall, the Bland-Altman plots had wide limits of agreement, which means the results are ambiguous and not acceptable for biomedical applications. However, data of the same subject has approximately the same bias in general. In the Bland-Altman plots of the maximum right shoulder abduction and maximum reaching distance, for data of the same subject the bias systematically changed for larger angles and reaching distance.

The inconsistency of biases between subjects and the underestimation may be due to the calibration step, in which the start and end have to be manually indicated per subject. These movements are used to define the sensor to segment orientation and the orientation in the global body frame. More time between these two movements would make recognition easier. Another possible explanation of the large errors is a not well adopted instructed posture during the calibration movements, which results in deviations between the measured joint angles and the real angles.

Other important sources for errors can be the sensor noise and sensor drift. For orientation estimation, a sensor fusion algorithm can be used. In this study, a Magdwick filter is applied for orientation estimation and compensates for the IMU inclination errors due to integration drift. The adjustable parameter β must

be high enough to minimize the errors due to integral drift, and low enough to prevent introducing unnecessary noise [20]. In this study, β was equal to 0.1. To find the most optimal value of β, data has to be processed with different values of β to compare the results and find the minimum offset at the beginning of the measurements.

For reaching distance, the acceleration has to be double integrated, leading to a large measurement error. The velocity drift is calculated assuming the velocity is zero at the beginning and end of the movement, and there is compensated for the integration drift by assuming constant noise. These compensation techniques can also have influence on the accuracy of the reaching distance.

Some technical problems were encountered during the exercise, namely loss of detection of the Vicon reflective markers. Occlusions of markers on the torso were gapfilled assuming the torso is a rigid body and thus ignoring breathing movements. Gaps on the upper limbs were filled using the Woltring quintic spline. This method is best for filling short gaps because it only uses the endpoints of the missing trajectory [30] These gap filling methods can result in low errors of marker positions [31] and can also have influence on the calculated metrics. To prevent marker occlusions, the camera positions must change and a transparent table to keep the markers in view must be used.

Altered soft tissue and skin artefacts can cause the IMUs to move with respect to the segments. However, in this low intensity exercises, the influence of these artefacts are negligible. During some exercises, the sensors came loose. This can result in another orientation than calculated, because the orientation of the IMUs is calculated in the sensor to segment calibration step and for defining the global frame. A solution for this would be better attachment of the IMUs.

4.2 Strengths and shortcomings

A few limitations of the study should be acknowledged when interpreting the results. The system was tested only with three participants that ware all female and relatively young. The subjects had body shapes, which can play a role in the sensor to segment step and for defining the global frame, because the body positions must be adapted perfectly. More subjects for testing the IMU system would result in better estimations of systematic and random biases [32].

This is the first study in the world that compares IMU based metrics during upper arm exercises with the Vicon Plug-in Gait as gold standard. The Plug-in Gait algorithm does not compute the angles on the same basis as the IMU algorithm, which can have affected the calculated shoulder abduction angles. In the Plug-in Gait algorithm, shoulder abduction is calculated relative to the thorax, in the IMU algorithm relative to the shoulder [18]. It would be interesting to calculate the shoulder abduction angle relative to the sternum IMU instead of the shoulder IMU.

Instead of IMUs, Magnetic, Angular Rate and Gravity (MARG) sensors can be used to provide a complete measurement of orientation relative to the direction of gravity and the earth's magnetic field to give a unique orientation of each sensor [20]. A disadvantage of MARGs is magnetic distortion that can be introduced by for example electrical appliances and metals for which must be compensated.

For the sensor to segment calibration step, only two movements are used, namely sitting straight (static) and trunk flexion (dynamic). Using the calibration movements as stated in table 2.2 and used in a prelimi-

nary study [12] may lead to a better and more reliable calibration, although in a clinical setting it takes more time to carry out.

In this study, the start and endpoint of reaching are determined manually. Wrong recognition of these points influences the different calculated metrics. It would be preferred to have a validated automatic detection of the start and endpoint of reaching.

Vicon markers were placed on soft tissue anatomical landmarks rather than attached to the IMUs. In this way, the motion analysis could be analysed [29]. A systematic underestimation of the angles and reaching distance for the IMU system was found. This was also found in other studies, placing the marks on landmarks rather than on the sensor [33]. This can be caused by the difference in position of the IMUs and the markers: the IMUs are placed more centrally on the segments, the markers more distally and thus undergoing larger angular displacements. To determine the absolute accuracy of the sensors and minimize the errors, the markers can also be placed on top of the IMU sensors.

4.3 Previous research

The findings of the current study do not support previous research from Bhagubai et al. [12]. In this study, the quality of some metrics was assumed to be acceptable based on trials performed on a rigid model of the arm and on healthy subjects, who were instructed to take some instructed positions with certain angles. The shoulder angles were measured with a standard deviation from the desired target from 3° in a rigid body model and 5° in healthy subjects. However, in this study, the accuracy of the IMUs was not determined with the gold standard, an optical motion system. Furthermore, in this study, a more extensive calibration was used for the sensor to segment step and the shoulder abduction angle was calculated by projecting $\vec{x_{ua}}$ to the zy-plane of the sternum's frame instead of the shoulder's frame. Despite that, to make the IMU system easy to set up at home, a simple system with as few IMUs and calibration steps as possible is preferred.

For the measurement of joint angle in the upper limb, wearable sensors are still in a developmental phase [17]. Previous studies compared other IMU devices to the gold standard VICON, in both healthy individuals and in other pathological conditions. However, different algorithms to process IMU signals were used, and different clinical variables were analysed. In a study from Poitras et al. ([32], the RMSE for trunk flexion varied from 1.8 to 5.9 ° and the correlation coefficient from 0.72 to 0.99. The shoulder abduction had an RMSE of 4.2 to 5.7 ° and a correlation coefficient from 0.72 to 0.91. In this study, it is emphasized that complex movements in two or three axes can account for the variability of results, because increasing movement complexity decreases the validity.

Fusion of data can enhance accuracy. In a review of Walmsley et al. [17] it was found that a multiple sensor fusion algorithms can be used for upper limb motion, but it is not clear which is best for specific joints or movements. Kalman filters can also be used to estimate the orientation of the human segment. However, a high sampling frequency is needed, and the filter has high computational costs. A Madgwick filter gives accurate results at lower sampling frequency and is better real time because of its low computational cost [34].

4.4 Recommendations

Further research should be undertaken to investigate the accuracy of the IMUs for reach-to-point movements, which also consider other arm activities and changes in the algorithm of the IMU system. More

focus on the sensor-fusion algorithm and the calibration is suggested. The present study is a necessary preliminary step before further research comparing IMUs to Vicon in CVA patients, although typical movements to mimic CVA patients have been investigated in this study. Using the IMUs in pathologic movement, can potentially introduce larger measurement errors for IMU based motion analysis.

Chapter 5

Conclusion

The aim of this study was to investigate the accuracy of trunk flexion, shoulder abduction and reaching distance measured with IMU sensors. The comparison demonstrated insufficient agreement between IMUs and Vicon, the gold standard for motion analysis. In general, metrics were underestimated by the IMU system. Correlation was variable for the metrics, as were the RMSE and MAE. Measurement accuracy could be subject to invalid calibration, sensor noise and drift. Notwithstanding the relatively limited sample size, this work offers valuable insights into the accuracy of the metrics measured with IMUs. The accuracy of IMUs for a reach-to-point movement in healthy adults must be further investigated and optimized before investigating the system in CVA patients.

Bibliography

[1] NHG-werkgroep Beroerte. *Beroerte*. Apr. 2018.

[2] Diji Kuriakose and Zhicheng Xiao. *Pathophysiology and Treatment of Stroke: Present Status and Future Perspectives*. 2020. DOI: 10.3390/ijms21207609.

[3] Eddie Kane and Nick S Ward. "Neurobiology of Stroke Recovery BT - Clinical Pathways in Stroke Rehabilitation: Evidence-based Clinical Practice Recommendations". In: ed. by Thomas Platz. Cham: Springer International Publishing, 2021, pp. 1–13. ISBN: 978-3-030-58505-1. DOI: 10.1007/978-3-030-58505-1{_}1.

[4] Thomas Platz and Mayowa Owolabi. "Clinical Pathways in Stroke Rehabilitation: Background, Scope, and Methods BT - Clinical Pathways in Stroke Rehabilitation: Evidence-based Clinical Practice Recommendations". In: ed. by Thomas Platz. Cham: Springer International Publishing, 2021, pp. 15–34. ISBN: 978-3-030-58505-1. DOI: 10.1007/978-3-030-58505-1{_}2.

[5] Samir R. Belagaje. "Stroke Rehabilitation". In: *CONTINUUM Lifelong Learning in Neurology* 23.1 (Feb. 2017), pp. 238–253. ISSN: 15386899. DOI: 10.1212/CON.0000000000000423.

[6] K L Ng and S T Carmichael. "Chapter 35 - Mechanisms of Stroke Recovery". In: ed. by Louis R Caplan et al. San Diego: Academic Press, 2017, pp. 171–174. ISBN: 978-0-12-803058-5. DOI: https://doi.org/10.1016/B978-0-12-803058-5.00035-7.

[7] Laura Miller McPherson and Julius P.A. Dewald. "Differences between flexion and extension synergy-driven coupling at the elbow, wrist, and fingers of individuals with chronic hemiparetic stroke". In: *Clinical neurophysiology : official journal of the International Federation of Clinical Neurophysiology* 130.4 (Apr. 2019), p. 454. ISSN: 18728952. DOI: 10.1016/J.CLINPH.2019.01.010.

[8] Angus J.C. McMorland, Keith D. Runnalls, and Winston D. Byblow. "A neuroanatomical framework for upper limb synergies after stroke". In: *Frontiers in Human Neuroscience* 9.FEB (Feb. 2015), p. 82. ISSN: 16625161. DOI: 10.3389/FNHUM.2015.00082/BIBTEX.

[9] Thomas Platz et al. "Arm Rehabilitation BT - Clinical Pathways in Stroke Rehabilitation: Evidence-based Clinical Practice Recommendations". In: ed. by Thomas Platz. Cham: Springer International Publishing, 2021, pp. 97–121. ISBN: 978-3-030-58505-1. DOI: 10.1007/978-3-030-58505-1{_}7.

[10] Yoon No Gregory Hong et al. "Are muscle synergies useful for stroke rehabilitation?" In: *Current Opinion in Biomedical Engineering* 19 (Sept. 2021), p. 100315. ISSN: 2468-4511. DOI: 10.1016/J.COBME.2021.100315.

[11] Anne Schwarz et al. "Systematic Review on Kinematic Assessments of Upper Limb Movements After Stroke". In: *Stroke* 50.3 (Mar. 2019), pp. 718–727. ISSN: 1524-4628. DOI: 10.1161/STROKEAHA.118.023531.

[12] Miguel M.C. Bhagubai et al. “Quantifying Pathological Synergies in the Upper Extremity of Stroke Subjects With the Use of Inertial Measurement Units: A Pilot Study”. In: *IEEE journal of translational engineering in health and medicine* 9 (Dec. 2020), p. 2100211. ISSN: 2168-2372. DOI: 10.1109/JTEHM.2020.3042931.

[13] Kathleen A. Lamkin-Kennard and Marko B. Popovic. “Sensors: Natural and Synthetic Sensors”. In: *Biomechatronics* (Jan. 2019), pp. 81–107. DOI: 10.1016/B978-0-12-812939-5.00004-5.

[14] Pablo MacEira-Elvira et al. “Wearable technology in stroke rehabilitation: Towards improved diagnosis and treatment of upper-limb motor impairment”. In: *Journal of NeuroEngineering and Rehabilitation* 16.1 (Nov. 2019), pp. 1–18. ISSN: 17430003. DOI: 10.1186/S12984-019-0612-Y/FIGURES/4.

[15] Riccardo Bravi et al. “An Inertial Measurement Unit-Based Wireless System for Shoulder Motion Assessment in Patients with Cervical Spinal Cord Injury: A Validation Pilot Study in a Clinical Setting”. In: *Sensors 2021, Vol. 21, Page 1057* 21.4 (Feb. 2021), p. 1057. ISSN: 1424-8220. DOI: 10.3390/S21041057.

[16] M. Saes et al. “Quantifying Quality of Reaching Movements Longitudinally Post-Stroke: A Systematic Review:” in: *https://doi.org/10.1177/15459683211062890* 2022.0 (Jan. 2022), p. 154596832110628. ISSN: 1545-9683. DOI: 10.1177/15459683211062890.

[17] Corrin P. Walmsley et al. “Measurement of Upper Limb Range of Motion Using Wearable Sensors: A Systematic Review”. In: *Sports Medicine - Open* 4.1 (Dec. 2018), pp. 1–22. ISSN: 21989761. DOI: 10.1186/S40798-018-0167-7/TABLES/4.

[18] Vicon. *Plug-in Gait Reference Guide*. Tech. rep. Vicon, 2021.

[19] Avinash Parnandi, Eric Wade, and Maja Matarić. “Motor function assessment using wearable inertial sensors”. In: *2010 Annual International Conference of the IEEE Engineering in Medicine and Biology Society, EMBC’10* (2010), pp. 86–89. DOI: 10.1109/IEMBS.2010.5626156.

[20] Sebastian O.H. Madgwick, Andrew J.L. Harrison, and Ravi Vaidyanathan. “Estimation of IMU and MARG orientation using a gradient descent algorithm”. In: *IEEE ... International Conference on Rehabilitation Robotics : [proceedings]* 2011 (2011). ISSN: 1945-7901. DOI: 10.1109/ICORR.2011.5975346.

[21] H.C. Theisens, D. Harborne, and T.J. Hesp. “7 CIMM Process Level IV - Creating Capable processes”. In: *Lean Six Sigma Green Belt Mindset, Skill set and Tool set*. 4th ed. Enschede: Lean Six Sigma Academy, 2020. Chap. 7 CIMM Pro, pp. 191–325. ISBN: 978-94-92240-06-4.

[22] Isabelle Poitras et al. “Validity and Reliability of Wearable Sensors for Joint Angle Estimation: A Systematic Review”. In: *Sensors 2019, Vol. 19, Page 1555* 19.7 (Mar. 2019), p. 1555. ISSN: 1424-8220. DOI: 10.3390/S19071555.

[23] Margit Alt Murphy, Carin Willén, and Katharina S. Sunnerhagen. “Responsiveness of upper extremity kinematic measures and clinical improvement during the first three months after stroke”. In: *Neurorehabilitation and Neural Repair* 27.9 (Nov. 2013), pp. 844–853. ISSN: 15459683. DOI: 10.1177/1545968313491008.

[24] Bernd J. Stetter et al. “A Machine Learning and Wearable Sensor Based Approach to Estimate External Knee Flexion and Adduction Moments During Various Locomotion Tasks”. In: *Frontiers in Bioengineering and Biotechnology* 8 (Jan. 2020), p. 9. ISSN: 22964185. DOI: 10.3389/FBIOE.2020.00009/BIBTEX.

[25] P. F. Watson and A. Petrie. “Method agreement analysis: A review of correct methodology”. In: *Theriogenology* 73.9 (June 2010), pp. 1167–1179. ISSN: 0093-691X. DOI: 10.1016/J.THERIOGENOLOGY.2010.01.003.

[26] J. Martin Bland and Douglas G. Altman. “STATISTICAL METHODS FOR ASSESSING AGREEMENT BETWEEN TWO METHODS OF CLINICAL MEASUREMENT”. In: *The Lancet* 327.8476 (Feb. 1986), pp. 307–310. ISSN: 0140-6736. DOI: 10.1016/S0140-6736(86)90837-8.

[27] Davide Giavarina. “Understanding Bland Altman analysis”. In: *Biochemia Medica* 25.2 (June 2015), pp. 141–151. ISSN: 13300962. DOI: 10.11613/BM.2015.015.

[28] Xavier Robert-Lachaine et al. “Validation of inertial measurement units with an optoelectronic system for whole-body motion analysis”. In: *Medical and Biological Engineering and Computing* 55.4 (Apr. 2017), pp. 609–619. ISSN: 17410444. DOI: 10.1007/S11517-016-1537-2/TABLES/3.

[29] Ryan Sers et al. “Validity of the Perception Neuron inertial motion capture system for upper body motion analysis”. In: (2019). DOI: 10.1016/j.measurement.2019.107024.

[30] Jonathan Camargo et al. “Automated gap-filling for marker-based biomechanical motion capture data”. In: *https://doi.org/10.1080/10255842.2020.1789971* 23 (2020), pp. 1180–1189. ISSN: 14768259. DOI: 10.1080/10255842.2020.1789971.

[31] Jakub Smolka and Edyta Lukasik. “The rigid body gap filling algorithm”. In: *Proceedings - 2016 9th International Conference on Human System Interactions, HSI 2016* (Aug. 2016), pp. 337–343. DOI: 10.1109/HSI.2016.7529654.

[32] Isabelle Poitras et al. “Validity and Reliability of Wearable Sensors for Joint Angle Estimation: A Systematic Review”. In: *Sensors 2019, Vol. 19, Page 1555* 19.7 (Mar. 2019), p. 1555. ISSN: 14248220. DOI: 10.3390/S19071555.

[33] Eric Allseits et al. “A Novel Method for Estimating Knee Angle Using Two Leg-Mounted Gyroscopes for Continuous Monitoring with Mobile Health Devices”. In: *Sensors 2018, Vol. 18, Page 2759* 18.9 (Aug. 2018), p. 2759. ISSN: 1424-8220. DOI: 10.3390/S18092759.

[34] Łukasz Leśniczek and Krzysztof Brzostowski. “Application of the sensor fusion for the system to track human upper limb motion”. In: *Advances in Intelligent Systems and Computing* 833 (2019), pp. 45–55. ISSN: 21945357. DOI: 10.1007/978-3-319-98678-4{_}7/FIGURES/7.

Appendix A

Marker placement

The marker set for the Plug-in Gait upper body was used (except the head), see table A.1[18].

Table A.1: Marker placement for Vicon. *Additional markers

Marker label	Definition	Position
Torso		
C7	7th cervical vertebra	Spinous process of the 7th cervical vertebra
T10	10th thoracic vertebra	Spinous process of the 10th thoracic vertebra
CLAV	Clavicle	Jugular notch where the clavicles meet the sternum
STRN	Sternum	Xiphoid process of the sternum
RBAK	Right back	Anywhere over the right scapula
Left upper limb		
LSHO	Left shoulder	Acromio-clavicular joint
LUPA	Left upper arm	Upper lateral 1/3 surface of the left arm
LELB	Left elbow	Lateral epicondyle
LFRM	Left forearm	Lower lateral 1/3 surface of the left forearm
LWRA	Left wrist marker A	Thumbside on the posterior of the left wrist, as close to the wrist joint center as possible
LWRB	Left wrist marker B	Little finger side on the posterior of the left wrist, as close to the wrist joint center as possible
LFIN	Left finger	Proximal to the middle knuckle on the left hand
LINDEX*	Left index	Top of the index finger
Right upper limb		
RSHO	Right shoulder	Acromio-clavicular joint
RUPA	Right upper arm	Upper lateral 1/3 surface of the right arm
RELB	Right elbow	Lateral epicondyle
RFRM	Right forearm	Lower lateral 1/3 surface of the right forearm
RWRA	Right wrist marker A	Thumbside on the posterior of the right wrist, as close to the wrist joint center as possible
RWRB	Right wrist marker B	Little finger side on the posterior of the right wrist, as close to the wrist joint center as possible
RFIN	Right finger	Proximal to the middle knuckle on the right hand
RINDEX*	Right index	Top of the index finger

Appendix B

Shoulder abduction and trunk flexion angles of all subjects

B.1 Subject 1 left

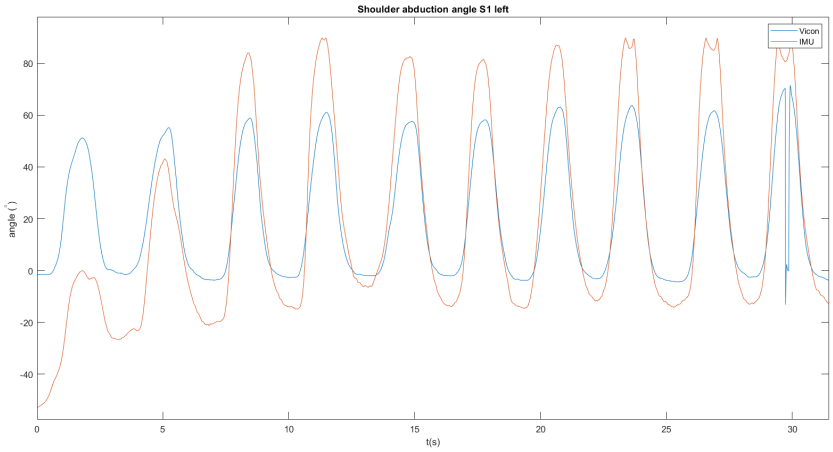

(a) Shoulder abduction angle

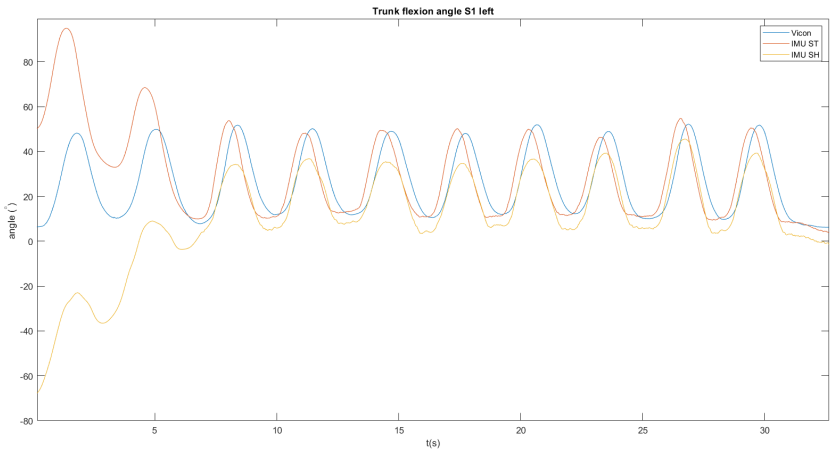

(b) Trunk flexion angle

Figure B.1: Shoulder abduction and trunk flexion angles of subject 1 during exercise 5 performed with left. Vicon data are in blue. IMU data are a) in red and b) in red (measured with ST) and yellow (measured with SH).

B.2 Subject 1 right

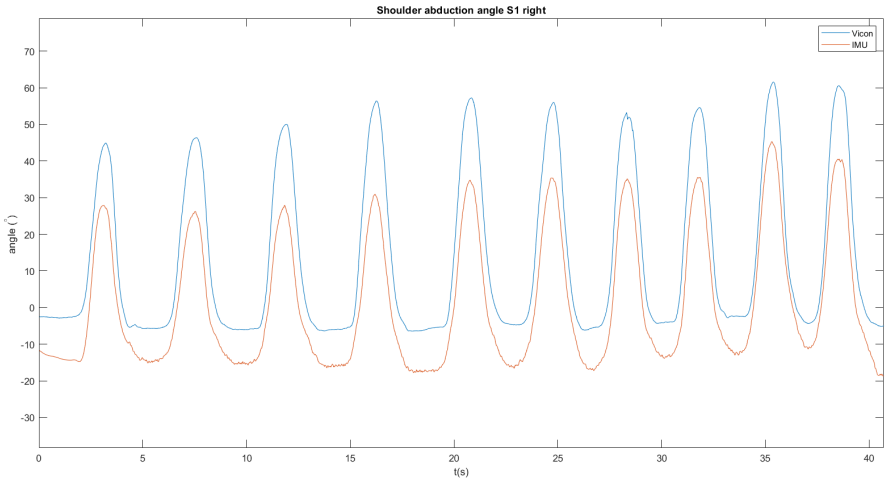

(a) Shoulder abduction angle

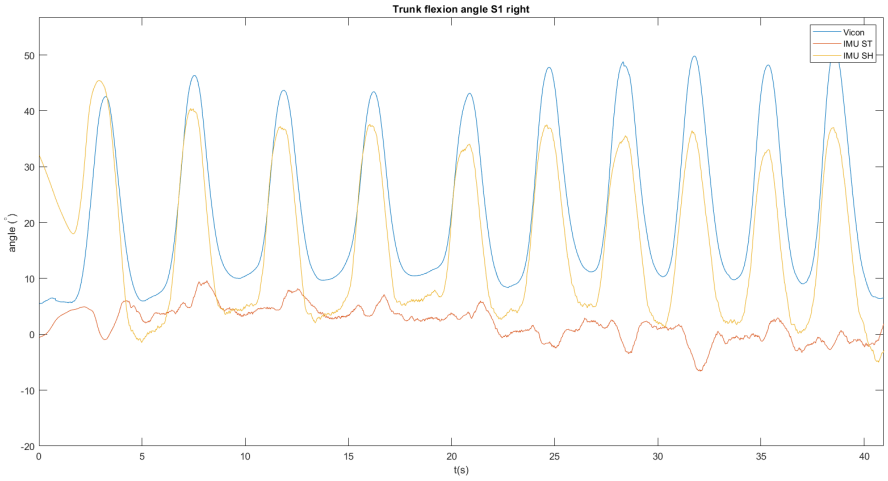

(b) Trunk flexion angle

Figure B.2: Shoulder abduction and trunk flexion angles of subject 1 during exercise 5 performed with right. Vicon data are in blue. IMU data are a) in red and b) in red (measured with ST) and yellow (measured with SH).

B.3 Subject 2 left

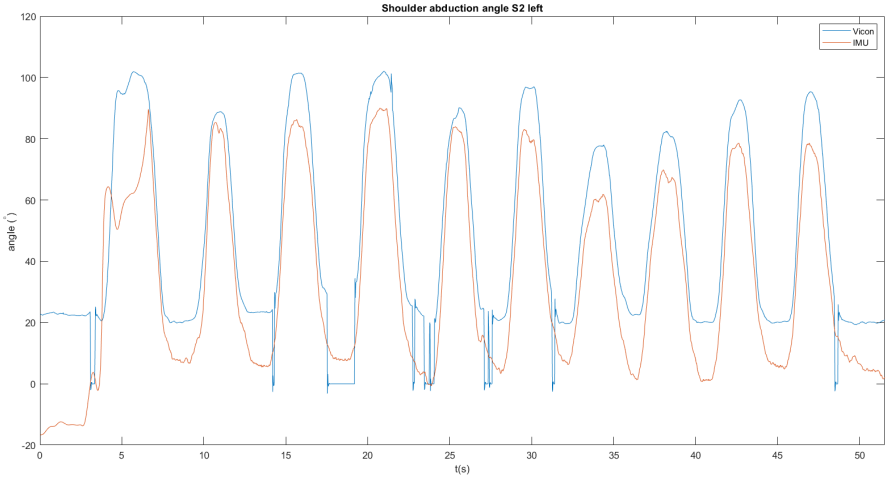

(a) Shoulder abduction angle

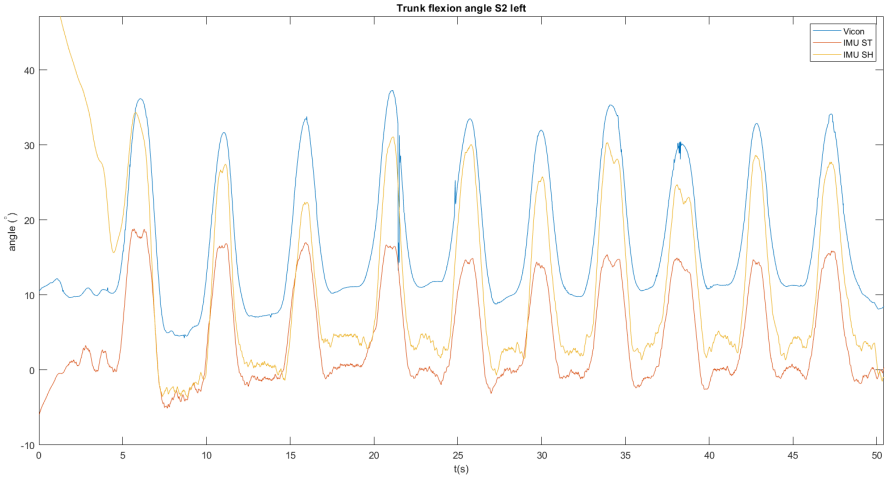

(b) Trunk flexion angle

Figure B.3: Shoulder abduction and trunk flexion angles of subject 2 during exercise 5 performed with left. Vicon data are in blue. IMU data are a) in red and b) in red (measured with ST) and yellow (measured with SH).

B.4 Subject 2 right

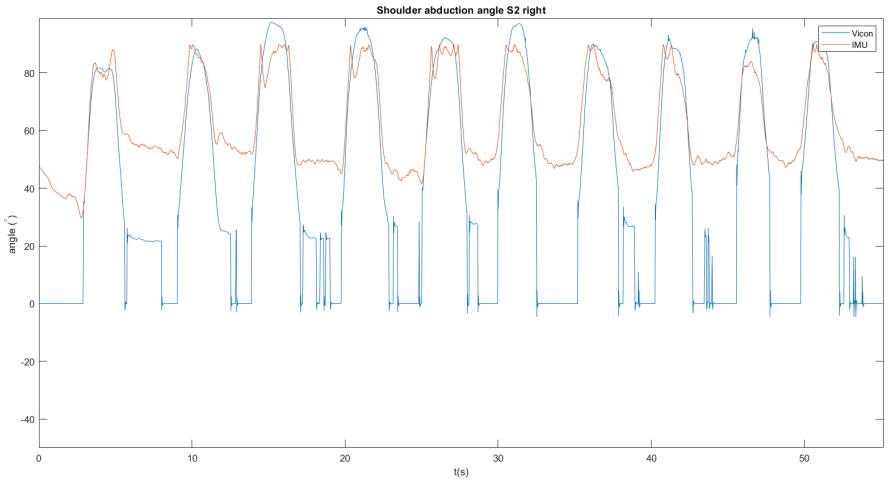

(a) Shoulder abduction angle

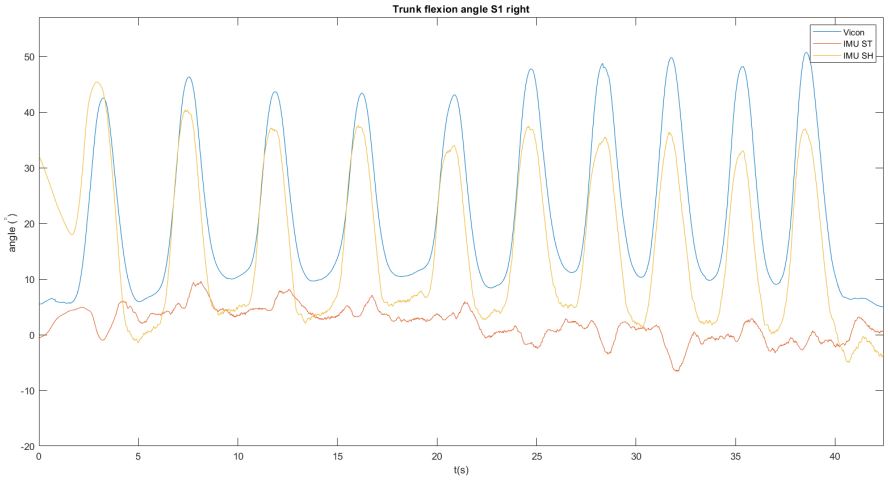

(b) Trunk flexion angle

Figure B.4: Shoulder abduction and trunk flexion angles of subject 2 during exercise 5 performed with right. Vicon data are in blue. IMU data are a) in red and b) in red (measured with ST) and yellow (measured with SH).

B.5 Subject 3 left

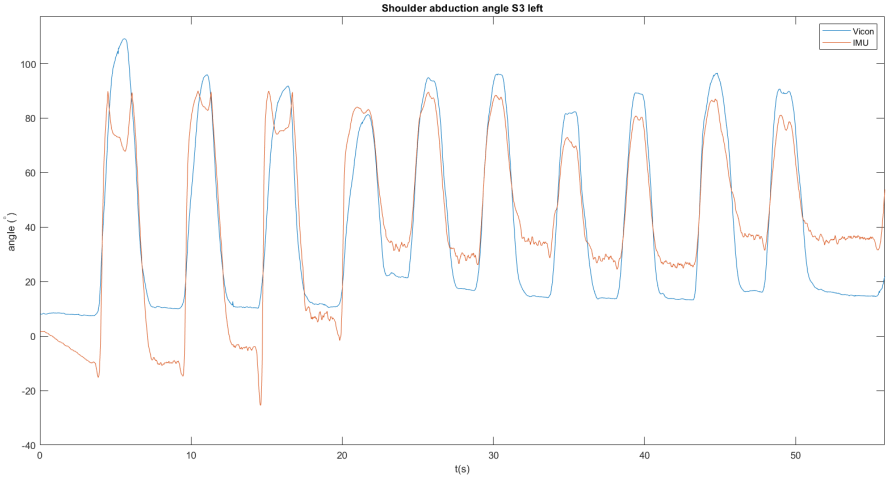

(a) Shoulder abduction angle

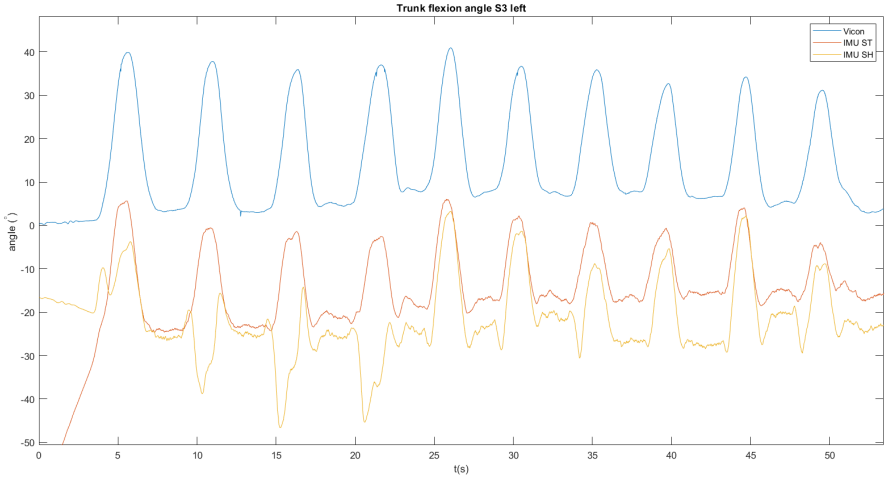

(b) Trunk flexion angle

Figure B.5: Shoulder abduction and trunk flexion angles of subject 3 during exercise 5 performed with left. Vicon data are in blue. IMU data are a) in red and b) in red (measured with ST) and yellow (measured with SH).

B.6 Subject 3 right

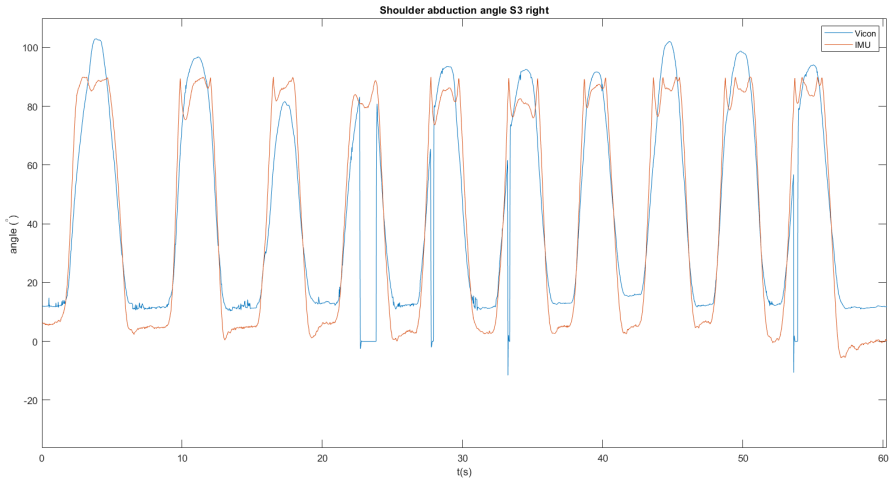

(a) Shoulder abduction angle

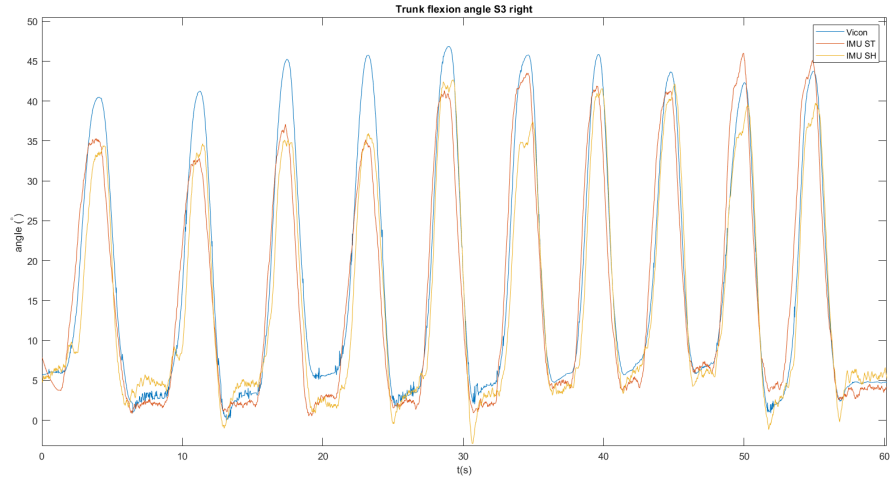

(b) Trunk flexion angle

Figure B.6: Shoulder abduction and trunk flexion angles of subject 3 during exercise 5 performed with right. Vicon data are in blue. IMU data are a) in red and b) in red (measured with ST) and yellow (measured with SH).